Single-molecule imaging for unravelling the functional diversity of 10-23 DNAzymes

Aida Montserrat Pagès[1,†], Mirjam Kümmerlin[2,3], Rebecca Andrews[2,‡], Achillefs N. Kapanidis[2,3,*], Dragana Spasic[1,§] and Jeroen Lammertyn[1,§,*]

1Department of Biosystems, Biosensors Group, KU Leuven - University of Leuven, 3001, Leuven, Belgium

2Biological Physics Research Group, Department of Physics, University of Oxford, OX1 3PU Oxford, United Kingdom

3Kavli Institute for Nanoscience Discovery, Dorothy Crowfoot Hodgkin Building, OX1 3QU, University of Oxford, Oxford, UK

ABSTRACT: DNA-based enzymes, also known as DNAzymes, have opened new opportunities for signal generation and amplification in several fields, including biosensing. However, biosensors performance can be hampered by heterogeneity in the catalytic activity of such DNAzymes, especially when relying on a limited number of molecules to generate signal. In this regard, single-molecule studies are essential to discern the behaviour among such heterogeneous molecules otherwise masked by ensemble measurements. This work presents a novel methodology to study the 10-23 RNA-cleaving DNAzyme at the single-molecule level. By means of measuring the distance-sensitive efficiency of Förster Resonance Energy Transfer using alternating-laser excitation on a super-resolution microscope, we determined the kinetics of individual DNAzymes in terms of substrate turnover, rate of the different reaction steps, and changes in performance over time. Our results revealed that, despite high concentrations of the reaction cofactor (i.e., Mg^{2+}), a maximum of only 70% of the DNAzymes are actively cleaving multiple substrate sequences; the DNAzyme molecules also showed a wide range of substrate turnover rates. Our findings shed new light on the functional diversity of DNAzymes and on the importance of exploring sequence modifications to improve their catalytic performance. Ultimately, this work presents a technique to obtain time-dependent information, which could be easily implemented to study other types of enzymes or biomolecular interactions.

Since the introduction of the first biosensor more than 60 years ago, the use of biosensors in diagnostics has been continuously growing, simultaneously pushing their boundaries in performance[1]. Over the years, biosensors have evolved towards platforms that can detect minute amounts of biomarkers[2–5]. In this context, one of the approaches to design such ultrasensitive biosensors has been based on dividing and encapsulating solutions in independent reaction chambers, with volumes typically in the femtoliter range, such as digital ELISA[6]. The majority of the digital ELISA concepts developed so far were based on proteins, showing, however, some limitations in terms of design flexibility[7].

Commonly, protein enzymes are employed for the generation of signal in digital ELISA, but RNA-cleaving deoxyribozymes (DNAzymes) offer an attractive alternative[8–10]. DNAzymes are single stranded DNA sequences capable of cleaving the phosphodiester bond between two RNA nucleotides[11,12] in the presence of their metal ion cofactors[12]. The potential of DNAzymes has been demonstrated by a wide variety of detection concepts for different target molecules and using different read-out strategies[13–18]. Thanks to their great specificity, DNAzymes have shown to be very valuable for multiplex target detection[19–21]. Moreover, when combined with the appropriate bioreceptor molecules, they can be used for simultaneous detection of heterogeneous targets (e.g., proteins and nucleic acids)[22]. In addition, DNAzymes offer several advantages compared to protein enzymes, such as stability in a wider range of conditions and the ability to work at different temperatures[23,24]. However, despite these advantages, their use in digital bioassays remains suboptimal due to the presence of heterogeneity among DNAzymes, which has significant impact when the bioassay performance relies on the activity of a limited number of DNAzyme molecules due to the low amounts of target in the solution.

In order to improve our understanding and the performance of DNAzymes in these settings, it is valuable to establish the levels of static heterogeneity among enzyme molecules[25]. Current approaches to study the catalytic performance of DNAzymes are mainly based on bulk measurements, which describe an average behaviour. Therefore, to gather information on heterogeneity, single-molecule (sm) measurements are needed[26]. To date, a number of studies have examined DNAzymes at the sm-level, mostly focusing on the relationship between the functionality and the structure of the DNAzyme, or the role of the metal ions[27,28]. More recently, J. Jung *et. al*. have reported the individual steps of a reaction cycle by monitoring changes of the distance between the ends of the DNAzyme sequence[29]. They observed that each cleavage cycle is divided in four steps: binding of the substrate to the DNAzyme, cleavage of the substrate, and subsequent dissociation of the two product strands. Nevertheless, the studies reported to date have looked at these different events separately and not as a sequence of events from the same DNAzyme, thus lacking the temporal aspect, which is essential for understanding the heterogeneity among molecules.

In this work, we introduce for the first time the study of the 10-23 DNAzyme cleavage reaction at the sm-level to determine the kinetics of individual DNAzymes, in terms of substrate turnover, rate of the different reaction steps and the changes in performance over time. This information is obtained by studying reaction trajectories and differentiating between cleavage and non-cleavage events, which in turn helps reveal functional differences among individual molecules. To achieve this objective, we use fluorescently labelled DNAzyme and substrate sequences (Figure 1A), and monitor their interaction by measuring the distance-sensitive efficiency of Förster Resonance Energy Transfer (FRET) using alternating-laser excitation (ALEX)[30] on a super-resolution microscope (Figure 1B). In the case of an interaction between the DNAzyme and the substrate, the two fluorophores used for labelling both molecules serve as the FRET donor (D) and the acceptor (A), respectively. The emissions of both the D and the A are simultaneously recorded for each field of view (Figure 1C). Employing the ALEX imaging mode, we monitor the presence of the substrate, and subsequently the product halves, regardless of the FRET efficiency (Figure 1D). Importantly, we monitor the cleavage activity of the DNAzyme under different reaction conditions, such as the concentration of the reaction cofactor (i.e., Mg^{2+}), and concentration of substrate. Subsequently, through the fitting of the fluorescent states for each channel (dashed lines in Figure 1D), we categorize the events for the different conditions to identify those corresponding to actual cleavage events (Figure 1E), which is used to calculate the percentage of active DNAzymes and the substrate turnover rates of individual DNAzymes, reporting on the diversity among molecules. Figure S1 in Supplementary information depicts the schematic representation of all the events identified. Furthermore, information about the rate constants is obtained for each reaction step. Finally, the DNAzyme reaction is monitored for a longer period of time to evaluate how the catalytic performance of DNAzymes changes over time.

This work depicts a novel approach to study enzymatic reactions at the sm-level, by employing the measurement of sequential events to gather evidence about the catalytic performance of DNAzymes. In this project, the 10-23 DNAzyme has been used as a model system, but this approach could be easily applied to other DNAzymes.

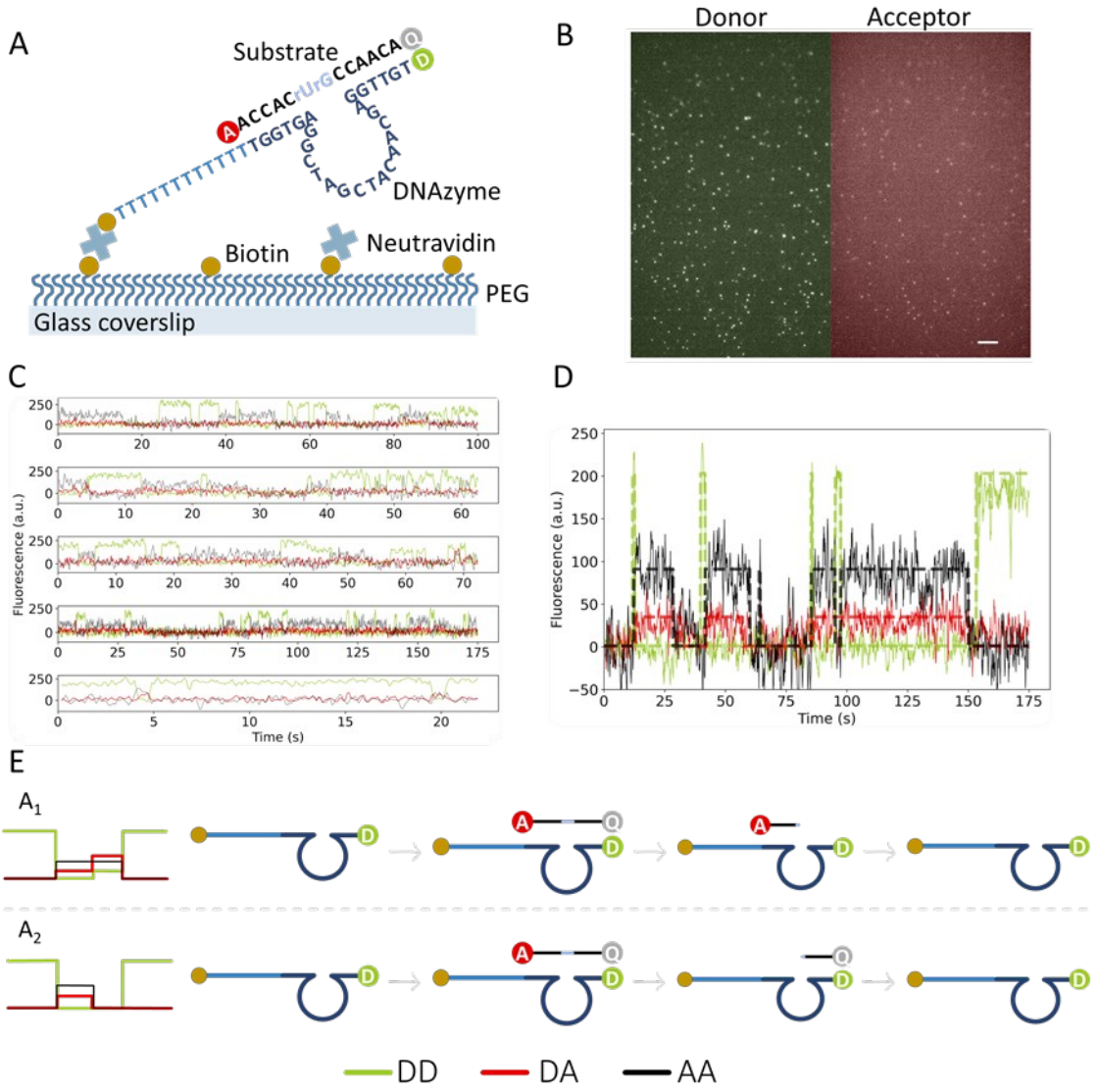

Figure 1. Schematic representation of the procedure to analyse and obtain the different events: **A)** The DNAzyme is biotinylated on one end (to enable immobilization to a PEG passivated glass surface through biotin-neutravidin binding) and labelled with the donor (D) on the other end, while the substrate is dually labelled with the acceptor (A) and a quencher (Q). **B)** The DNAzyme reaction is recorded with Nanoimager S fluorescence microscope and each field of view is split into two halves, displaying the emission of both the D and A channels. Scale bar = 5 µm. **C)** For each individual DNAzyme, the fluorescence changes over time are extracted using an in-house built software (GapViewer)[31]. Then, the fluorescent channels are split based on the emission of the D and the A (the latter upon excitation of the D), represented by DD (green) and DA (red), while the emission of the A upon direct excitation is depicted by AA (black). **D)** The fluorescence states for each channel (solid lines) are fitted with ebFRET software[32] (dashed lines). Individual events are defined as the fluorescent state changes in between two DD high signal state. Then, based on the sequence of fluorescence state changes, several types of events are identified. **E)** Schematic representation of the events identified within the time traces that refer to cleavage of the substrate

MATERIALS AND METHODS

Reagents

The oligonucleotides used in this work (Figure 1A) were purchased from Integrated DNA Technologies (IDT, Leuven, Belgium) and used without further purification. Vectabond was obtained from Vector Labs (California, USA), and the silicone gaskets from Grace Bio-Labs (Oregon, USA). Polyethylene-glycol (PEG) was acquired from Laysan Bio (Alabama, USA), and phosphate-buffered saline (PBS) and glucose oxidase from Sigma Aldrich (UK). Catalase was purchased from Roche Diagnostics (Germany), and neutravidin was obtained from ThermoFisher Scientific (UK).

Microscope coverslip preparation

Glass coverslips, which have been heated at 500 °C for 1 h, were immersed in a solution containing 1 % (v/v) Vectabond in acetone for 10 min. Then, the coverslips were rinsed with acetone and water, and dried with nitrogen. A silicon gasket with four reaction chambers was placed on top of the coverslip. Next, the reaction chambers were passivated with 20 µL of a solution containing 235 mg/mL of PEG-SVA and 7.7 mg/mL of biotin-PEG in 0.1 M $NaHCO_3$, for 1.5 h. Finally, the slides were washed three times with 200 µL of 1X PBS and stored at 4 °C covered with PBS.

Sample preparation

Before the measurement, each reaction chamber in the coverslip was incubated with 20 µL of 0.5 mg/mL Neutravidin in 0.5X PBS for 10 min, followed by three washing steps with 200 µL of 1X PBS. Next, 20 µL of 100 pM biotinylated DNAzyme in MilliQ water was incubated for 30 s, followed by three washing steps with 200 µL of 1X PBS Then, 20 µL of substrate was added in imaging buffer (50 mM KCl, 20 mM $MgCl_2$ in 10 mM Tris-HCl (pH 8.3), together with 1 mM TROLOX, 1 % Glucose, 40 µg/mL catalase and 0.1 mg/mL glucose oxidase).

Instrumentation/movie acquisition

sm-fluorescence movies were recorded using the Nanoimager S fluorescence microscope (Oxford Nanoimaging, ONI, Oxford, United Kingdom). The data was collected with the objective-based total internal reflection fluorescence (TIRF) illumination mode, at an illumination angle of 53.5°. All the measurements were performed at standard room temperature (RT, i.e., 20-25 °C). The recording was performed using ALEX mode, with excitation laser powers of 3.6 mW at 532 nm, and 0.61 mW at 640 nm, Figure 1B. For all the experiments, 50 ms exposure was used, and unless stated otherwise, all fields of view were recorded for 400 s.

Data analysis

The recorded movies were processed with the home-built software GapViewer to extract the fluorescent time traces of individual DNAzymes (Figure 1C)[31]. Only traces that could be attributed to one single DNAzyme were manually selected for further analysis.

After removing the photobleached frames, the fluorescent channels were separated based on the green and red channel upon green excitation (DD and DA, respectively), and the red channel upon red excitation (AA). Then, the three fluorescent channels were fitted using Hidden Markov Modelling (HMM) with the ebFRET software (Figure 1D)[32]. The DD and DA channels were fitted with three different fluorescence states, and the AA channel, with two.

Next, based on the sequence of fluorescence state changes, several types of events were identified. Employing an in-house developed Python script, the states of the three fluorescent channels were simultaneously analysed for each individual trace to identify the events. More detailed information about the states of the events and the corresponding molecular sequence can be found in Figure 1E and Figure S1 in Supplementary information.

The analysis of the data was performed in Python 3.7, (scripts publicly available, see Availability section), and the histograms were plotted using Origin (OriginLab).

RESULTS AND DISCUSSION

Categorization of the events

To monitor the 10-23 DNAzyme reaction at RT, we used the re-engineered DNAzyme strand reported by Ven *et al*[33]. This DNAzyme sequence was (1) modified with a 3’ biotin to enable immobilization on the glass surface, (2) extended with a sequence of 15 thymine (T) nucleotides to give some flexibility and (3) labelled with 5’ Cy3, a fluorophore used for localizing it on the surface (Figure 1A) and for serving as a FRET donor. The DNAzyme substrate was dually labelled with the 5’ Cy5 fluorophore (serving as FRET acceptor) and a 3’ Dabcyl quencher (indicated as Q)[34,35]. The functionality of the labelled DNAzyme was confirmed in bulk by monitoring the product generation over time and compared with a non-labelled DNAzyme. For this test, we used a substrate dually labelled with FAM on the 5’-end and a Q (Iowa Black® FQ quencher) on the 3’-end. Only a small decrease in the signal generated (~9 %) was observed compared to the unmodified DNAzyme sequence (Figure S2), which was attributed to possible interferences between the two fluorescent labels (FAM and Cy3 on the substrate and DNAzyme, respectively) rather than differences in the activity of the DNAzyme.

The DNAzyme-catalysed reaction was monitored at the sm-level on a passivated glass surface by means of objective-based TIRF microscopy (Figure 1A). The dual labelling of the substrate together with the ALEX imaging mode allowed us to differentiate events based on the observed emission and sequence of emissions from the fluorophores (Figure S3). The binding of a substrate is detected by a drop in $D_{excitation}$-$D_{emission}$ (DD) intensity, induced by the Q getting in close proximity to the D fluorophore. This is accompanied by signal increase, some signal in the $D_{excitation}$-$A_{emission}$ (DA) and $A_{excitation}$-$A_{emission}$ (AA) channel.

Upon cleavage, the product half carrying the Q leaves, inducing a rise of DA intensity (due to FRET), followed by the dissociation of the product half carrying the A, which can restore the DD intensity to the former level (event type A1, see Figure 1E). Alternatively, the half carrying the A leaves first, which results in loss of both the DA and AA signal, and after unbinding of the product half with the Q, the DD signal is restored (event

A2, see Figure 1E). Experimental examples of these events can be found in Figure S4 and S5. Moreover, the analysis of multiple individual time traces showed additional events which were assumed as non-cleavage events (I_1-I_3, with schematic explanation in Figure S1, and experimental examples in Figure S6 and S7). Notably, event classification relies on the fitting of the fluorescent states, and on an in-house developed program that looks for specific sequences of such fluorescent states (Figure 1D).

In order to verify that the events defined as cleavage were actual cleavage events, we compared the events identified in the absence of Mg^{2+} and with those measured with higher concentrations of Mg^{2+}, up to 100 mM. To ensure enough events for statistical analysis, we used a fixed concentration of 100 nM of substrate. As can be seen in Figure 2A, the non-cleavage events (I_1-I_3) comprised an 80 % of the total events measured in the absence of Mg^{2+}. Across all Mg^{2+} concentrations used, the overall percentage of events that were cleavage events (A_1 and A_2) on average was 50 %. The results indicated a statistical difference only between 0 mM Mg^{2+} and the Mg^{2+} concentrations equal or higher than 2 mM (Table S1), suggesting that the different Mg^{2+} concentrations (i.e., 10, 20, 60 and 100 mM) can, overall, promote more events per DNAzyme (both cleavage and non-cleavage events), as depicted by the increase of the ratio between the total number of events and the total number of DNAzymes (Table S2).

Another important element of the reaction is the ratio of the substrate and DNAzyme concentrations, as large ratios between the two could affect the DNAzyme performance. Hence, we screened several concentrations of the substrate ranging from 10 to 400 nM, with the upper limit determined by the background fluorescence. For these experiments, 20 mM of Mg^{2+} was selected, as it is the most commonly used concentration when working with DNAzymes[22,36–38], and also no significant differences were observed in the percentage of the event types for higher Mg^{2+} concentrations. Similar to the previous measurements, we quantified all the events to calculate the percentage of which were cleavage events. We observed that for increasing substrate concentrations, DNAzymes undergo more events overall (Table S2), but the percentage of events which were cleavage events (sum of A_1 and A_2) remains constant (Figure 2B) with the only statistical difference between 50 nM and the highest tested concentration (400 nM) (Table S3). Moreover, for 400 nM, a decrease of the overall percentage of the cleavage events (A_1 and A_2) is noticeable together with an increase of the I_3 non-cleavage event. Based on the definition of I_3 event, a possible hypothesis could be that, due to the large concentration of substrate in the solution, two different substrates are able to bind to a single DNAzyme, one on each substrate-binding arm (Figure S1), thereby prohibiting cleavage of the substrate and decreasing the availability of active DNAzyme on the surface.

Next, we focused on individual DNAzymes and color-coded the cleavage (orange) and non-cleavage events (blue). Figure S8 and S9 illustrate examples for the screening of two Mg^{2+} concentrations and two substrate concentrations, respectively. Each row represents one DNAzyme in the field of view, and the different lines within each row, refer to an event. As expected and already described, the substrate and Mg^{2+} concentration had a big impact on the mean number of events observed. Based in the observed number of traces on the y-axis, there is a substantial increase in the number of DNAzymes undergoing events when increasing the concentration of Mg^{2+} and substrate. Moreover, based on the number of events on the x-axis, and as also seen in Table S2, the higher the concentration of Mg^{2+} and the substrate, the larger the number of events (cleavage and non-cleavage) a DNAzyme engages in. Furthermore, the results revealed that there is a pronounced variability on productivity of different DNAzyme molecules, particularly observable among the DNAzymes with a large number of overall events. These results led to the assumption that a certain number of DNAzymes might not partake in any cleavage event, which can be observed from the rows with just blue lines.

To test our hypothesis, we calculated the number of events within a trace and grouped the traces based on the number of different events observed (no cleavages, only one cleavage, and multiple cleavage events). We found that the percentage of DNAzymes with multiple cleavage events increased with increasing Mg^{2+} concentration (Figure 2E). Nevertheless, for every Mg^{2+} concentration tested, we observed that at least 20% of the DNAzymes showed no cleavage activity or only one cleavage event, hereinafter referred as inactive DNAzymes. Such results could be explained by different aspects interfering with the reaction, such as a non-optimal conformation of the DNAzyme-substrate complex, steric hindrance between the immobilized sequence and the glass surface, or errors in DNA sequences during their synthesis. The statistical analysis performed on the traces displaying multiple cleavages indicated a significant difference (at least a 37 %) between the lowest Mg^{2+} concentrations (i.e., 0 and 2 mM) and almost all the concentrations in the range from 10 to 100 mM (the detailed information can be found in Table S5). However, unexpectedly we also observed significant decrease in active DNAzymes for 60 mM, and 20 and 100 mM. These results are in line with the slightly lower percentage of A_1 and A_2 (40 %) in Figure 2A, but more research is needed to formulate a hypothesis.

With regard to the substrate concentration (Figure 2F), a clear statistical difference was observed for the lowest concentration (10 nM), which mainly showed one cleavage event per trace, compared to the higher concentrations which are mainly characterised by traces with multiple events (Table S6). These results can be explained by the limited number of substrate molecules in the solution for 10 nM. Thus, the activity of the DNAzyme is affected more by the diffusion of the substrate molecules resulting in a slower hybridization rate[35]. While for higher concentrations of substrate we observed a comparable percentage of active DNAzymes (i.e., DNAzymes showing multiple cleavages), we also noticed that at least 20% of the DNAzymes were inactive. Based on these findings we could infer that some of the sequences are not able to adopt the necessary conformation for cleavage, as suggested by the structural variability of the core observed in the work of Borggräfe *et. al.*[39]. Interestingly, by only looking at the cleavage events, we observed that DNAzymes are not able to perform many cleavages consecutively. As can be seen in the examples from Figure S8 and S9, in many instances, we noticed only one or two cleavage events in a row (consecutive blue lines). Nevertheless, favourable reaction conditions, such as larger concentrations of Mg^{2+}, promoted more cleavage events in a row.

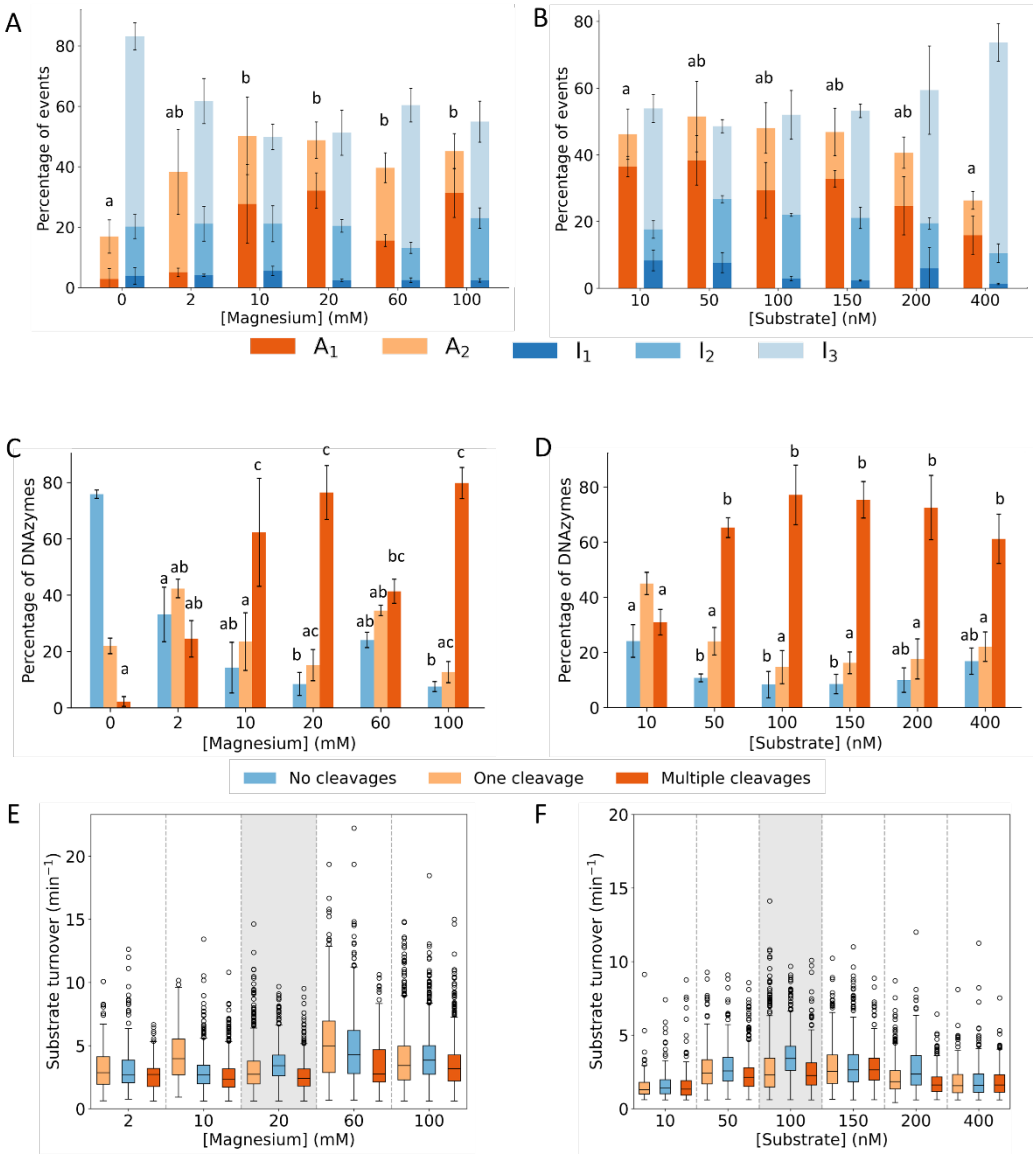

Figure 2. Overview of the cleavage events and catalytic performance for individual DNAzymes: **A)** Categorization of the events identified for different concentrations of Mg^{2+}, at a fixed substrate concentration of 100 nM. **B)** Categorization of the events identified for several substrate concentrations, at a fixed Mg^{2+} concentration of 20 mM. For a more correct visualization and comparison, percentages are used, but the absolute values can be found in Table S2. **C)** Classification of the DNAzyme traces based on the number of cleavage events for different concentrations of Mg^{2+} at a fixed substrate concentration of 100 nM. **D)** Classification of the DNAzyme traces based on the number of cleavage events for several concentrations of substrate in the presence of 20 mM of Mg^{2+}. For a accurate correct visualization and comparison, percentages are used, absolute

values can be found in Table S4 **E)** Boxplot representing the substrate turnover for several concentrations of Mg^{2+} (2 – 100 mM) and a substrate concentration of 100 nM. **F)** Boxplot representing the substrate turnover for various concentrations of substrate (10 - 400 nM) at 20 mM Mg^{2+} concentration. In panels G and H, the different colours represent the three independent repetitions and the grey shaded area refers to the matching experimental conditions (e.g., 20 mM of Mg^{2+} and 100 nM of substrate) between the two screenings. The error bars depict one standard deviation of three repetitions. In panels A-D, the means with a common letter are not significantly different based on a Tukey test (alpha = 0.5). For A and B panels, the same lettering holds for both groups.

Substrate turnover rate

From the analysis performed so far, we observed an overall increase in the number of cleavage events when increasing the concentration of Mg^{2+} and/or substrate. Nevertheless, such analysis was based on comparing the events of all the DNAzymes together. To have more insight in the enzymatic capabilities of individual DNAzymes, we calculated the substrate turnover rate - number of substrate molecule conversions per time unit - per DNAzyme. We did not find any statistical difference on the average substrate turnover when increasing the concentration of Mg^{2+} (Figure 2E, Table S7). However, the increase of the interquartile range together with the larger width of the distributions (Figure S10) we concluded that the higher the Mg^{2+} concentration, the higher the chances of having faster DNAzymes. Focusing on the substrate screening (Figure 2F), the average turnover increased with the concentration of substrate, no significant differences could be determined (Table S8), reaching a plateau at 100 nM. As also mentioned before, the turnover for the lowest concentrations could be limited by the stability of the hybridization between the substrate and DNAzyme. Moreover, as depicted by the size of the interquartile range, the activity of DNAzymes at low concentrations is more homogeneous. Interestingly, for 400 nM, the substrate turnover decreased substantially, which was associated with the significant decrease of the percentage of cleavage events (Figure 2B). Also, as can be seen in Figure S11, the average substrate turnover is within the same order of magnitude. However, the higher the concentration of substrate, the narrower the distribution, indicating that the DNAzyme cannot achieve such fast substrate turnover rates. Overall, the width of the distributions, together with large interquartile ranges, suggested considerable functional heterogeneity among DNAzymes. The cleavage of a substrate requires the proper folding of the DNAzyme-substrate complex, the binding of multiple Mg^{2+}, and a series of sequential proton transfer steps[39,40]. Hence, any deviation from one of the steps could result in significant changes. Additionally, as the DNAzymes are immobilized, differences in the microenvironment could also affect the performance.

Kinetic analysis

The findings from the substrate turnover analysis indicated that both the concentration of Mg^{2+} and substrate influence the performance of the reaction. To further characterise this dependence we calculated the dwell time, which refers to the duration of a specific step, for both the time in between events and duration of each event (Figure 3A). For each event, a histogram of the frequency count was fitted with a single exponential decay (Figure 3B)[35]. Regarding the on-rate (k_{on}), which refers to the rate of association between the substrate and the DNAzyme (Figure 4), we naturally observed faster association rates when increasing the concentration of both Mg^{2+} and substrate (Figure 3C and 3D). The results of the linear range obtained from this analysis (dashed lines in Figure 3C and 3D) were compared with the rate constants estimated from ensemble data using the model developed in-house (Table S9)[41]. Interestingly, using the same DNAzyme sequence and concentration of Mg^{2+}, we noticed that the dependence of k_{on} on the substrate at the sm-level was ~4-fold lower. Considering the rates from the reaction in bulk were obtained from measurements in solution and the sm rates from immobilized DNAzymes, the lower k_{on} for sm DNAzymes could be a consequence of the repulsive electrostatic forces from the surface[35].

Next, we focused on the different reaction steps and calculated the rate of each step. For the cleavage events, we observed that the rate constant of the first half of the event (subpanels i and iii in Figure 3E and F) was three times slower than for the second half (subpanels ii and iv in Figure 3E and F). To interpret these differences, we should take into account that the first step involves several reaction steps that cannot be discerned with the used labelling approach, including the cleavage of the phosphodiester bond, the conformational changes required for cleavage, and the release of the first product strand. During that time period, the DNAzyme structure was locked and stabilized for the cleavage to take place, thus the complex should undergo conformational changes before the sequences can be released[39]. Therefore, the rate constant obtained refers to the slowest of all these steps. Comparing the ensemble rate constants obtained with the in-house model (k_{clv} in Table S9), the rate constants are within the same order of magnitude with those of the first half of the event, indicating that the values from subpanels i and iii in Figure 3E and F are in reference to cleavage step. Then, focusing on the second step of the event, i.e., the

release of second half, we observed similar dissociation kinetics for both product halves (subpanels ii and iv in Figure 3E and F), suggesting comparable stability. Additionally, based on the results from Figure 2A and 2B, we obtained a larger percentage of A_1 events, suggesting that the product labelled with the Q is dissociating first. We hypothesized that this preference could be related with the structural conformation of the complex. According to the most favoured structure of the precatalytic complex derived by Borggräfe *et. al.*[39], this half of the substrate is on the outer part of the structure.

Concerning events I_1-I_3, based on the rates (Figure S12), it seems that they represent unsuccessful cleavages, with some heterogeneity. The comparison between the rates obtained for I_2 (Figure S12A-ii) with the first step of the cleavage events (Figure 3A-i and 3B-i) revealed similar kinetics. This would mean that the dissociation rate of the non-cleaved substrate is in the same order as the first step of cleavage, which could give an indication for the low substrate turnover rates. Nevertheless, the information obtained with these experiments is insufficient to reveal further details. Interestingly, we noticed that for I_2, which refers to the dissociation of the substrate without cleavage (Figure S1), the rate for 60 mM was higher compared to the other concentrations (Figure S12A-ii). This change in the kinetics could be a possible explanation for the differences in the percentage of active DNAzymes observed in Figure 2E. Finally, the dissociation rate constant of the substrate obtained with the model in bulk is in accordance with the values obtained in this work.

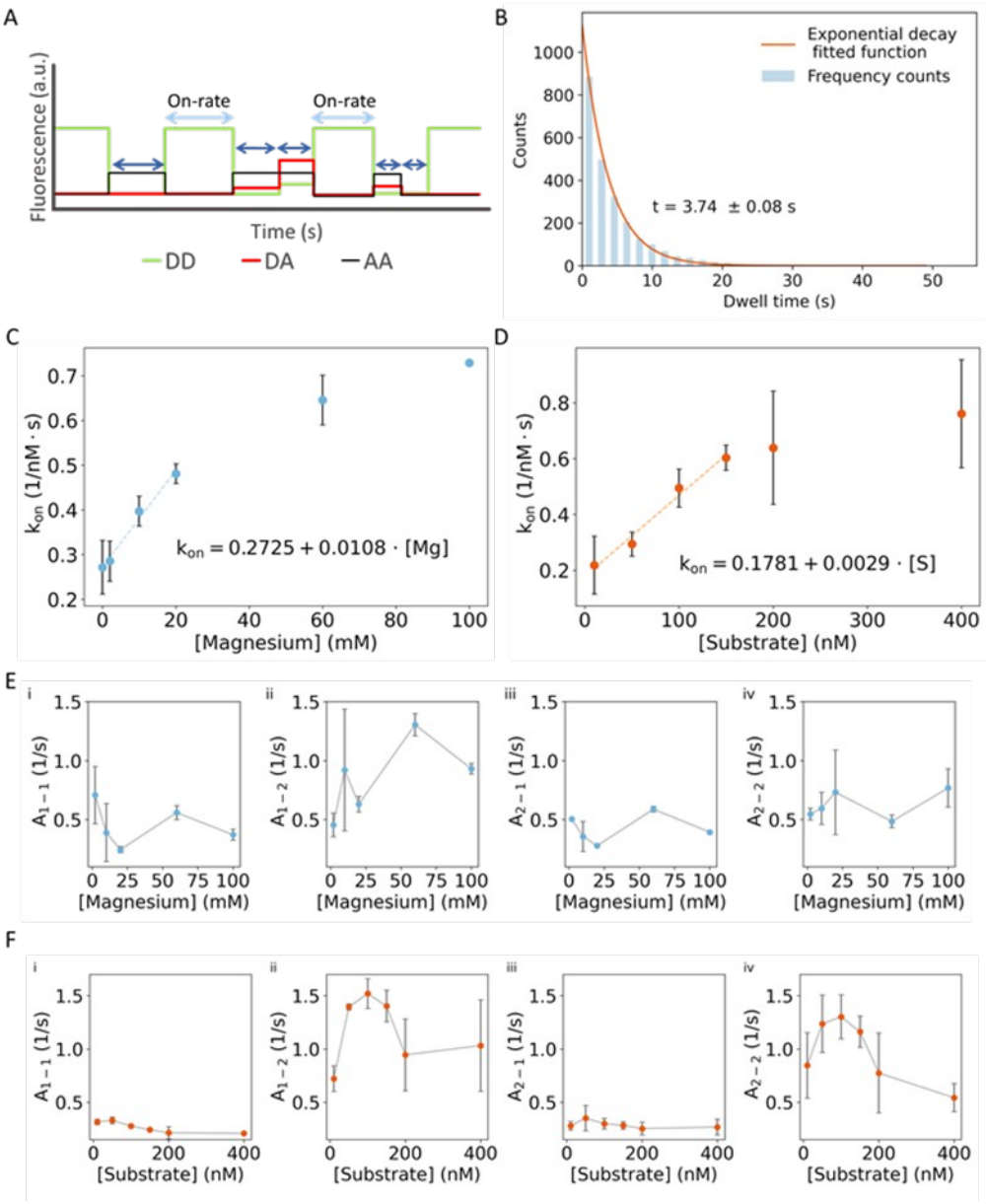

Figure 3. Kinetic analysis **A)** Schematic representation of an example trace depicting how the dwell times are obtained. The interval of time in between events (light blue) is used to calculate the on-rate and the time

period of the steps within one event are grouped (dark blue). **B)** A frequency count of the dwell times is plotted for each event separately, and the resulting histogram is fitted with a single exponential decay (n = 2384). **C)** Concentration-dependent response of the on-rate for several concentrations of Mg^{2+} (0 – 100 mM) at a fixed substrate concentration of 100 nM. The dashed line depicts the linear range with the corresponding equation. **D)** Concentration-dependent response of the on-rate for several concentrations of substrate (10 – 400 nM) at a fixed Mg^{2+} concentration of 20 mM. The dashed line depicts the linear range with the corresponding equation. **E**) Rate of individual reaction steps for the cleavage events (A_1 and A_2) for a range of Mg^{2+} concentrations from 2 to 100 mM at 100 nM of substrate. A schematic representation of the cleavage events can be found in Figure 1E. **F**) Rate of individual reaction steps for the cleavage events (A_1 and A_2) for a range of substrate concentrations from 10 to 400 nM at a fixed Mg^{2+} concentration of 20 mM. Since events A_1 and A_2 consist of two steps, separate graphs are depicted for each of them, where subpanels i and ii correspond to A_1, while subpanels iii and iv refer to A_2. The error bars depict one standard deviation of three independent repetitions.

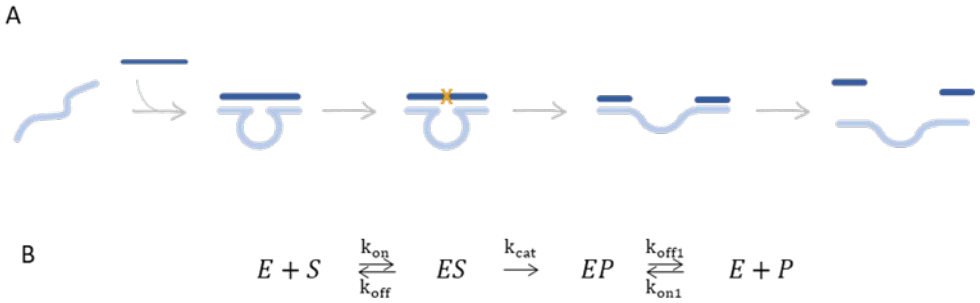

Figure 4. Reaction mechanism of the 10-23 DNAzyme illustrated **A)** schematically and **B)** by the minimal kinetic scheme, respectively. DNAzymes (E) contain two substrate binding arms, adjacent to the catalytic core, which bind the substrate (S). The hybridization of E and S forms a complex (ES), which cleaves the phosphodiester bond between the RNA bases positioned in the middle of the substrate sequence (depicted in A with an orange cross), resulting in EP. After cleavage, the catalytic core stretches, increasing the end-to-end distance. Subsequently, the product sequences are released, and E is able to initiate a new reaction. In this kinetic scheme, P refers to the product strand that dissociates most slowly. The reaction is monitored by labelling the ends of the S with a fluorophore (F) and a quencher (Q). Upon cleavage of the S sequence, the distance between the F and Q increases resulting in a fluorescent signal increase. The association and dissociation of E and S are indicated by k_{on} and k_{off}. The cleavage rate is defined by k_{clv}, and the rate for release and binding of P are represented by k_{rls} and k_{bin}

DNAzyme performance over time

From the biosensor development point of view, it is desirable for an enzyme to work at its maximal cleavage rate for as long as possible. To gather this information about the DNAzymes, we monitored the activity of individual DNAzymes over 30 min. For this set of experiments, we selected the reaction conditions that promoted the highest cleavage and percentage of active DNAzymes (100 nM of substrate and 100 mM of Mg^{2+}). Since it was not possible to measure a single field of view for such long period of time due to photobleaching of the fluorescent labels on the surface, we recorded twelve different fields of view, each for 2.5 min, in the same reaction chamber. The whole surface was in contact with the substrate solution, thus all DNAzymes in the surface were carrying out reactions in spite of not being measured. Following the same analysis methodology as described previously (Figure 1), we quantified the percentage of active DNAzymes for the different time points. As can be seen in Figure 5A, no statistically significant difference (Table S10) was observed for measurement times over the time monitored. Similarly, comparing the percentage of inactive DNAzymes after 2 and 30 min (Figure 5B), we observed no significant differences among the different time points (Table S11).

In order to get information about whether the catalytic activity of a DNAzyme is affected over time, we calculated the substrate turnover rate of individual DNAzymes and compared them for the different time points. Based on the results obtained (Figure 5C), we could infer that the DNAzyme are able to maintain a steady catalytic power for reaction times within 30 min.

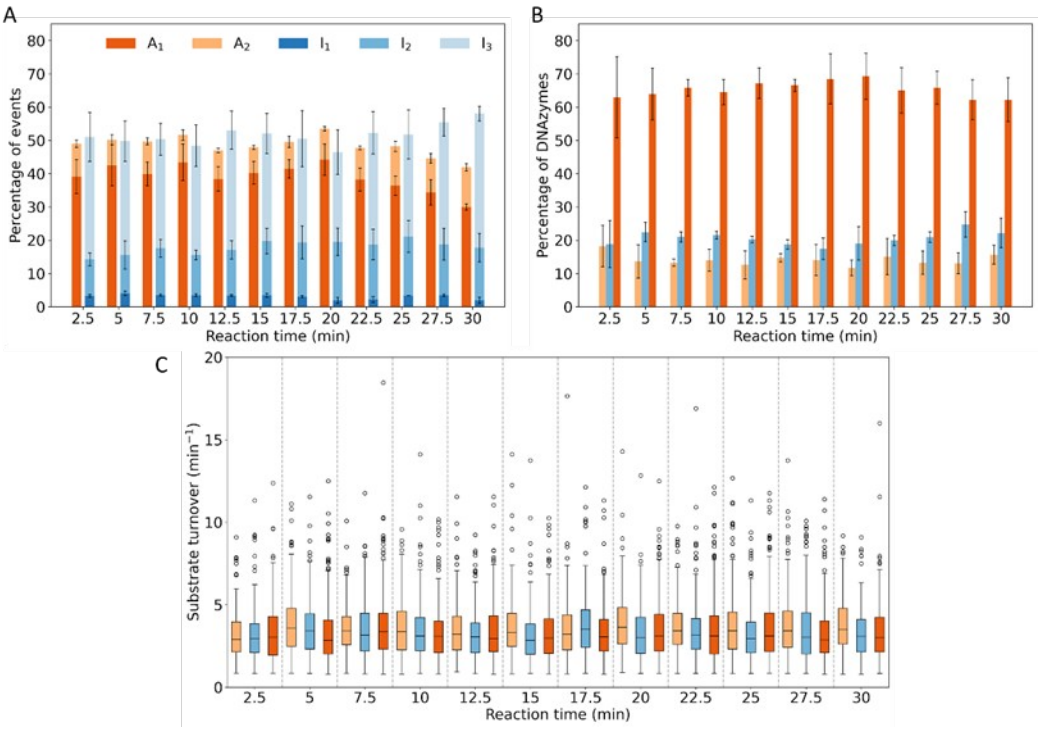

Figure 5. Evaluation of the DNAzyme catalytic performance over time: **A)** Percentage of events for the different identified categories. **B)** Percentage of traces based on the number of executed cleavage events**. C)** Evolution of the substrate turnover over time. The reaction time depicted in the x-axis refers to the different fields of view of the same surface measured sequentially. The different colours represent the three independent repetitions. The error bars depict one standard deviation of three repetitions.

CONCLUSIONS

The main goal of this work was to study the functional heterogeneity of DNAzymes by determining the substrate turnover of individual DNAzyme molecules tethered to a glass surface. To achieve this, we established an analysis procedure to differentiate between cleavage and non-cleavage events. By quantifying the number of actual cleavage events for each individual DNAzymes, we calculated the percentage of active DNAzymes, which refers to DNAzymes cleaving at least two substrates during the measurement time.

Despite increasing the concentrations of the reaction cofactor and the availability of substrate, we observed that approximately 20 % of the DNAzymes were able to perform only one or no cleavages. Also, the distributions of the calculated substrate turnovers showed a particularly broad range of values. These results denoted the significant heterogeneity among DNAzyme sequences.

Moreover, we showed that large ratios between the DNAzyme and the substrate can hinder the performance, possibly due to competitive inhibition. This was evidenced by the substantial decrease of cleavage events and substrate turnover at high substrate concentrations. Finally, we demonstrated that DNAzymes are able to sustain uniform cleavage capabilities for a period of time beyond 30 min.

The findings reported here shed new light on the functional diversity of DNAzymes, and the possible challenges when developing applications relying on a limited number of DNAzymes, like in digital bioassays. In view of the fact that some studies have explored sequence modifications to improve the catalytic performance of DNAzymes[42,43], future research could employ the analysis strategy introduced in this study to evaluate the impact of these modifications on the percentage of active DNAzyme or the variance of substrate turnover. Notwithstanding, the methodology presented in this work is not specific for DNAzymes but can be employed to systematically study and optimize any other enzymatic reaction or multistep molecular interactions at the sm-level.

ASSOCIATED CONTENT

Supporting Information

- Schematic representation of the different events
- Summary tables with the number of events for each category
- Distribution of the substrate turnover and the corresponding fittings
- Concentration-dependent kinetic curve

- Results for the DNAzyme performance over time measurements.

Availability

The scripts upon which this study is based are openly available in https://github.com/AiidaMP/DNAzyme-single-molecule

AUTHOR INFORMATION

Corresponding Author

* Jeroen Lammertyn. Tel: +32 16321459; e-mail: jeroen.lammertyn@kuleuven.be, ORCID: 0000-0001-8143-6794
* Achillefs N. Kapanidis. Tel: +44 1865 272 226; e-mail: a.kapanidis1@physics.ox.ac.uk, ORCID: 0000-0001-6699-136X

Present Addresses

†FOx Biosystems, BioVille, Agoralaan Abis, 3590 Diepenbeek, Belgium
‡ Department of Chemistry, University of Zurich, Winterthurerstrasse 190, 8057, Zurich, Switzerland

Author Contributions

All authors have given approval to the final version of the manuscript. ‡§These authors contributed equally.

Funding Sources

This work has received funding from European Union's Horizon 2020 research and innovation programme under the Marie Skłodowska-Curie grant agreement No 675412 (H2020-MSCAITN-ND4ID), KU Leuven (C32/15/005) and the Fund for Scientific Research Flanders (G082522N, IDN/21/006). This work was also supported by the Wellcome Trust (110164/Z/15/Z to A.N.K.), two UK EPSRC studentships (to M.K. and R.A.), and a doctoral fellowship of the Boehringer Ingelheim Fonds (to M.K.).

Conflict of interest disclosure

The work was performed using miniaturised commercial microscopes from Oxford Nanoimaging, a company in which A.N.K. is a co-founder and shareholder.

REFERENCES

(1) Patil, S. B.; Annese, V. F.; Cumming, D. R. S. Commercial Aspects of Biosensors for Diagnostics and Environmental Monitoring. *Adv. Nanosensors Biol. Environ. Anal.* **2019**, 133–142. https://doi.org/10.1016/B978-0-12-817456-2.00008-5.

(2) Giljohann, D. A.; Mirkin, C. A. Drivers of Biodiagnostic Development. *Nat. 2009 4627272* **2009**, *462* (7272), 461–464. https://doi.org/10.1038/nature08605.

(3) Kelley, S. Biomolecular Sensors: Benchmarking Basics. *ACS Sensors* **2016**, *1* (12), 1380. https://doi.org/10.1021/ACSSENSORS.6B00775/ASSET/IMAGES/MEDIUM/SE-2016-00775G_0001.GIF.

(4) Kelley, S. O.; Mirkin, C. A.; Walt, D. R.; Ismagilov, R. F.; Toner, M.; Sargent, E. H. Advancing the Speed, Sensitivity and Accuracy of Biomolecular Detection Using Multi-Length-Scale Engineering. *Nat. Publ. Gr.* **2014**. https://doi.org/10.1038/NNANO.2014.261.

(5) Wu, Y.; Tilley, R. D.; Gooding, J. J. Challenges and Solutions in Developing Ultrasensitive Biosensors. *J. Am. Chem. Soc.* **2018**, *141* (3), 1162–1170. https://doi.org/10.1021/JACS.8B09397.

(6) Zhang, Y.; Noji, H. Digital Bioassays: Theory, Applications, and Perspectives. *Anal. Chem.* **2017**, *89* (1), 92–101. https://doi.org/10.1021/ACS.ANALCHEM.6B04290/ASSET/IMAGES/LARGE/AC-2016-04290Z_0005.JPEG.

(7) Spindel, S.; Sapsford, K. E. Evaluation of Optical Detection Platforms for Multiplexed Detection of Proteins and the Need for Point-of-Care Biosensors for Clinical Use. *Sensors* **2014**, *14*, 22313–22341. https://doi.org/10.3390/s141222313.

(8) Safdar, S.; Ven, K.; van Lent, J.; Pavie, B.; Rutten, I.; Dillen, A.; Munck, S.; Lammertyn, J.; Spasic, D. DNA-Only, Microwell-Based Bioassay for Multiplex Nucleic Acid Detection with Single Base-Pair Resolution Using MNAzymes. *Biosens. Bioelectron.* **2020**, *152*. https://doi.org/10.1016/j.bios.2020.112017.

(9) Zhang, T.; Liu, C.; Zhou, W.; Jiang, K.; Yin, C.; Zhang, Z.; Li, H. Ultrasensitive Detection of Pb 2+ Based on a DNAzyme and Digital PCR. **2019**. https://doi.org/10.1155/2019/3528345.

(10) Zhu, P.; Shang, Y.; Tian, W.; Huang, K.; Luo, Y.; Xu, W. Ultra-Sensitive and Absolute Quantitative Detection of Cu2+ Based on DNAzyme and Digital PCR in Water and Drink Samples. *Food Chem.* **2017**, *221*, 1770–1777. https://doi.org/10.1016/J.FOODCHEM.2016.10.106.

(11) Santoro, S. W.; Joyce, G. F. A General Purpose RNA-Cleaving DNA Enzyme. *Biochemistry* **1997**, *94* (9), 4262–4266. https://doi.org/10.1073/pnas.94.9.4262.

(12) Rosenbach, H.; Victor, J.; Etzkorn, M.; Steger, G.; Riesner, D.; Span, I. Molecular Features and Metal Ions That Influence 10-23 DNAzyme Activity. *Molecules* **2020**, *25* (13). https://doi.org/10.3390/molecules25133100.

(13) Peeters, B.; Safdar, S.; Daems, D.; Goos, P.; Spasic, D.; Lammertyn, J. Solid-Phase PCR-Amplified DNAzyme Activity for Real-Time FO-SPR Detection of the MCR-2 Gene. *Anal. Chem.* **2020**, *92* (15), 10783–10791. https://doi.org/10.1021/acs.analchem.0c02241.

(14) Wei, L.; Wang, X.; Wu, D.; Li, C.; Yin, Y.; Li, G. Proximity Ligation-Induced Assembly of DNAzymes for Simple and Cost-Effective Colourimetric Detection of Proteins with High Sensitivity. *Chem. Commun.* **2016**, *52* (32), 5633–5636. https://doi.org/10.1039/c6cc00205f.

(15) Yan, Y.; Ma, C.; Tang, Z.; Chen, M.; Zhao, H. A Novel Fluorescent Assay Based on DNAzyme-Assisted Detection of Prostate Specific Antigen for Signal Amplification. *Anal. Chim. Acta* **2020**, *1104* (4), 172–179. https://doi.org/10.1016/j.aca.2020.01.014.

(16) Wang, G.; Chu, L. T.; Hartanto, H.; Utomo, W. B.; Pravasta, R. A.; Chen, T. H. Microfluidic Particle Dam for Visual and Quantitative Detection of Lead Ions. *ACS Sensors* **2020**, *5* (1), 19–23.

(17) Yun, W.; Li, N.; Wang, R.; Yang, L.; Chen, L.; Tang, Y. Proximity Ligation Assay Induced Hairpin to DNAzyme Structure Switching for Entropy-Driven Amplified Detection of Thrombin. *Anal. Chim. Acta* **2019**, *1064* (8), 104–111.

(18) Jiang, K.; Wu, Y.; Chen, J.; Shi, M.; Meng, H. M.; Li, Z. Molecular Recognition Triggered Aptazyme Cascade for Ultrasensitive Detection of Exosomes in Clinical Serum Samples. *Chinese Chem. Lett.*

2021, *32* (5), 1827–1830. https://doi.org/10.1016/j.cclet.2020.11.031.

(19) Zhang, L.; Guo, S.; Zhu, J.; Zhou, Z.; Li, T.; Li, J.; Dong, S.; Wang, E. Engineering DNA Three-Way Junction with Multifunctional Moieties: Sensing Platform for Bioanalysis. *Anal. Chem.* **2015**, *87* (22), 11295–11300. https://doi.org/10.1021/acs.analchem.5b02468.

(20) Zhou, W.; Liang, W.; Li, D.; Yuan, R.; Xiang, Y. Dual-Color Encoded DNAzyme Nanostructures for Multiplexed Detection of Intracellular Metal Ions in Living Cells. **2016**. https://doi.org/10.1016/j.bios.2016.05.058.

(21) Li, C.; Ma, J.; Shi, H.; Hu, X.; Xiang, Y.; Li, Y.; Li, G. Design of a Stretchable DNAzyme for Sensitive and Multiplexed Detection of Antibodies. *Anal. Chim. Acta* **2018**, *1041*, 102–107. https://doi.org/10.1016/j.aca.2018.08.052.

(22) Montserrat Pagès, A.; Safdar, S.; Ven, K.; Lammertyn, J.; Spasic, D. DNA-Only Bioassay for Simultaneous Detection of Proteins and Nucleic Acids. *Anal. Bioanal. Chem.* **2021**, *413* (20), 4925–4937. https://doi.org/10.1007/S00216-021-03458-6/TABLES/2.

(23) Silverman, S. K. Catalytic DNA: Scope, Applications, and Biochemistry of Deoxyribozymes. *Trends Biochem. Sci.* **2016**, *41* (7), 595–609. https://doi.org/10.1016/j.tibs.2016.04.010.

(24) Ma, L.; Liu, J. Catalytic Nucleic Acids: Biochemistry, Chemical Biology, Biosensors, and Nanotechnology. *iScience* **2020**, *23* (1), 100815. https://doi.org/10.1016/J.ISCI.2019.100815.

(25) Liebherr, R. B.; Renner, M.; Gorris, H. H. A Single Molecule Perspective on the Functional Diversity of in Vitro Evolved β-Glucuronidase. *J. Am. Chem. Soc.* **2014**, *136* (16), 5949–5955. https://doi.org/10.1021/ja412379p.

(26) Kapanidis, A. N.; Strick, T. Biology, One Molecule at a Time. *Trends in Biochemical Sciences*. 2009, pp 234–243. https://doi.org/10.1016/j.tibs.2009.01.008.

(27) Jung, J.; Han, K. Y.; Koh, H. R.; Lee, J.; Choi, Y. M.; Kim, C.; Kim, S. K. Effect of Single-Base Mutation on Activity and Folding of 10-23 Deoxyribozyme Studied by Three-Color Single-Molecule ALEX FRET. *J. Phys. Chem. B* **2012**, *116* (9), 3007–3012. https://doi.org/10.1021/jp2117196.

(28) Kim, H. K.; Rasnik, I.; Liu, J.; Ha, T.; Lu, Y. Dissecting Metal Ion-Dependent Folding and Catalysis of a Single DNAzyme. *Nat. Chem. Biol.* **2007**, *3* (12), 763–768. https://doi.org/10.1038/nchembio.2007.45.

(29) Jung, J.; Kim, S. Y.; Kim, S. K. Single-Molecule Study of the Effects of Temperature, PH, and RNA Base on the Stepwise Enzyme Kinetics of 10–23 Deoxyribozyme. *RSC Adv.* **2022**, *12* (23), 14883–14887. https://doi.org/10.1039/D2RA02131E.

(30) Kapanidis, A. N.; Laurence, T. A.; Nam, K. L.; Margeat, E.; Kong, X.; Weiss, S. Alternating-Laser Excitation of Single Molecules. *Acc. Chem. Res.* **2005**, *38* (7), 523–533. https://doi.org/10.1021/AR0401348/ASSET/IMAGES/LARGE/AR0401348F00008.JPEG.

(31) Sow, M.; Steuer, H.; Adekanye, S.; Ginés, L.; Mandal, S.; Gilboa, B.; Williams, O. A.; Smith, J. M.; Kapanidis, A. N. High-Throughput Nitrogen-Vacancy Center Imaging for Nanodiamond Photophysical Characterization and PH Nanosensing. *Nanoscale* **2020**, *12* (42), 21821–21831. https://doi.org/10.1039/d0nr05931e.

(32) Van De Meent, J. W.; Bronson, J. E.; Wiggins, C. H.; Gonzalez, R. L. Empirical Bayes Methods Enable Advanced Population-Level Analyses of Single-Molecule FRET Experiments. *Biophys. J.* **2014**, *106* (6), 1327–1337. https://doi.org/10.1016/j.bpj.2013.12.055.

(33) Ven, K.; Safdar, S.; Dillen, A.; Spasic, D.; Lammertyn, J. Re-Engineering 10–23 Core DNA- and MNAzymes for Applications at Standard Room Temperature. *Anal. Bioanal. Chem.* **2018**, *411* (1), 205–215. https://doi.org/10.1007/s00216-018-1429-4.

(34) Kümmerlin, M.; Mazumder, A.; Kapanidis, A. N. Fluorescence and FRET Based on Fluorogenic and Transient DNA Binding. https://doi.org/10.1002/cphc.202300175.

(35) Andrews, R. DNA Hybridisation Kinetics Using Single-Molecule Fluorescence Imaging. *Essays Biochem.* **2021**, *65* (1), 27–36. https://doi.org/10.1042/ebc20200040.

(36) Mokany, E.; Bone, S. M.; Young, P. E.; Doan, T. B.; Todd, A. V. MNAzymes, a Versatile New Class of Nucleic Acid Enzymes That Can Function as Biosensors and Molecular Switches. *J. Am. Chem. Soc.* **2010**, *132* (3), 1051–1059. https://doi.org/10.1021/ja9076777.

(37) Yuan, B. F.; Xue, Y.; Luo, M.; Hao, Y. H.; Tan, Z. Two DNAzymes Targeting the Telomerase MRNA with Large Difference in Mg 2+ Concentration for Maximal Catalytic Activity. *Int. J. Biochem. Cell Biol.* **2007**, *39* (6), 1119–1129. https://doi.org/10.1016/j.biocel.2007.03.004.

(38) Gao, J.; Shimada, N.; Maruyama, A. MNAzyme-Catalyzed Nucleic Acid Detection Enhanced by a Cationic Copolymer. *Biomater. Sci.* **2015**, *3* (5), 716–720. https://doi.org/10.1039/c4bm00449c.

(39) Borggräfe, J.; Victor, J.; Rosenbach, H.; Viegas, A.; Gertzen, C. G. W. W.; Wuebben, C.; Kovacs, H.; Gopalswamy, M.; Riesner, D.; Steger, G.; Schiemann, O.; Gohlke, H.; Span, I.; Etzkorn, M. Time-Resolved Structural Analysis of an RNA-Cleaving DNA Catalyst. *Nature* **2022**, *601* (May 2021), 144–149. https://doi.org/10.1038/s41586-021-04225-4.

(40) Breaker, R. R.; Emilsson, G. M.; Lazarev, D.; Nakamura, S.; Puskarz, I. J.; Roth, A.; Sudarsan, N. A Common Speed Limit for RNA-Cleaving Ribozymes and Deoxyribozymes. *RNA* **2003**, *9* (8), 949–957. https://doi.org/10.1261/RNA.5670703.

(41) Montserrat Pagès, A.; Hertog, M.; Nicolaï, B.; Spasic, D.; Lammertyn, J. Unraveling the Kinetics of the 10–23 RNA-Cleaving DNAzyme. *International Journal of Molecular Sciences*. 2023. https://doi.org/10.3390/ijms241813686.

(42) Yu, T.; Zhou, W.; Liu, J. An RNA-Cleaving Catalytic DNA Accelerated by Freezing. *ChemBioChem* **2018**, *19* (10), 1012–1017. https://doi.org/10.1002/cbic.201800049.

(43) Gao, J.; Shimada, N.; Maruyama, A. Enhancement of Deoxyribozyme Activity by Cationic Copolymers. *Biomater. Sci.* **2015**, *3* (2), 308–316.

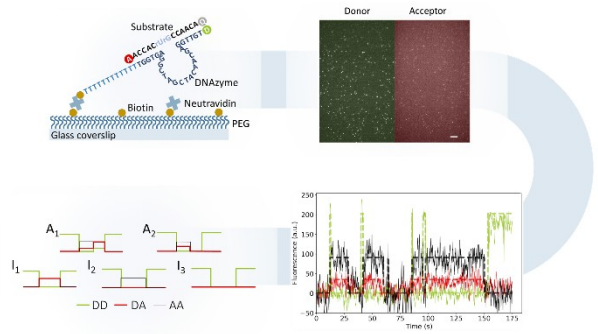
Substrate
DNAzyme
Biotin
Neutravidin
PEG
Glass coverslip
Donor
Acceptor
A1
A2
I1
I2
I3
DD
DA
AA
Time (s)